Received: 20 February 2018 | Revised: 8 April 2018 | Accepted: 9 April 2018

DOI: 10.1111/gcb.14287

PRIMARY RESEARCH ARTICLE

WILEY Global Change Biology

Cross-scale controls on carbon emissions from boreal forest megafires

Xanthe J. Walker[1] | Brendan M. Rogers[2] | Jennifer L. Baltzer[3] | Steven G. Cumming[4] | Nicola J. Day[3] | Scott J. Goetz[1,2,5] | Jill F. Johnstone[6] | Edward A. G. Schuur[1] | Merritt R. Turetsky[7] | Michelle C. Mack[1]

[1]Center for Ecosystem Science and Society, Northern Arizona University, Flagstaff, Arizona

[2]Woods Hole Research Center, Falmouth, Massachusetts

[3]Biology Department, Wilfrid Laurier University, Waterloo, Ontario, Canada

[4]Department of Wood and Forest Sciences, Laval University, Quebec City, Quebec, Canada

[5]School of Informatics, Computing and Cyber Systems (SICCS), Northern Arizona University, Flagstaff, Arizona

[6]Department of Biology, University of Saskatchewan, Saskatoon, Saskatchewan, Canada

[7]Department of Integrative Biology, University of Guelph, Guelph, Ontario, Canada

Correspondence
Xanthe J. Walker, Center for Ecosystem Science and Society, Northern Arizona University, Flagstaff, AZ.
Email: xanthe.walker@gmail.com

Funding information
NASA Arctic Boreal and Vulnerability Experiment (ABoVE), Grant/Award Number: Legacy Carbon Grant: #Mack-01; Division of Environmental Biology, Grant/Award Number: RAPID grant #1542150; Government of the Northwest Territories Cumulative Impacts Monitoring Program Funding, Grant/Award Number: #170; NSERC Discovery Grant; Polar Knowledge Canada's Northern Science Training Program

Abstract

Climate warming and drying is associated with increased wildfire disturbance and the emergence of megafires in North American boreal forests. Changes to the fire regime are expected to strongly increase combustion emissions of carbon (C) which could alter regional C balance and positively feedback to climate warming. In order to accurately estimate C emissions and thereby better predict future climate feedbacks, there is a need to understand the major sources of heterogeneity that impact C emissions at different scales. Here, we examined 211 field plots in boreal forests dominated by black spruce (*Picea mariana*) or jack pine (*Pinus banksiana*) of the Northwest Territories (NWT), Canada after an unprecedentedly large area burned in 2014. We assessed both aboveground and soil organic layer (SOL) combustion, with the goal of determining the major drivers in total C emissions, as well as to develop a high spatial resolution model to scale emissions in a relatively understudied region of the boreal forest. On average, 3.35 kg C m^{-2} was combusted and almost 90% of this was from SOL combustion. Our results indicate that black spruce stands located at landscape positions with intermediate drainage contribute the most to C emissions. Indices associated with fire weather and date of burn did not impact emissions, which we attribute to the extreme fire weather over a short period of time. Using these results, we estimated a total of 94.3 Tg C emitted from 2.85 Mha of burned area across the entire 2014 NWT fire complex, which offsets almost 50% of mean annual net ecosystem production in terrestrial ecosystems of Canada. Our study also highlights the need for fine-scale estimates of burned area that represent small water bodies and regionally specific calibrations of combustion that account for spatial heterogeneity in order to accurately model emissions at the continental scale.

KEYWORDS
black spruce, carbon combustion, fire severity, jack pine, *Picea mariana*, *Pinus banksiana*, taiga plains, taiga shield

1 | INTRODUCTION

As global environmental change intensifies, there is an increasing need to predict ecological responses to these changes at scales that are larger than the plot, landscape, or even ecoregion—hereafter macroscales (Heffernan et al., 2014). One macroscale feedback mechanism of increasing importance to the climate-carbon cycle is wildfire in carbon-rich areas such as the boreal biome. Globally, the

boreal forest stores approximately 40% of terrestrial carbon (C) and has historically been considered a C sink (Bradshaw & Warkentin, 2015; Pan et al., 2011). However, recent climate warming and drying has led to an intensification of large wildfires, particularly in the boreal forests of northwestern North America (Kasischke et al., 2010). Increased combustion associated with this changing fire regime could shift this region of the boreal forest from a C sink to a C source (Bond-Lamberty, Peckham, Ahl, & Gower, 2007), which would act as a positive feedback to climate warming (Li, Lawrence, & Bond-Lamberty, 2017; Randerson et al., 2006). Understanding the processes that determine C emissions at different scales would indicate where and when such changes from sink to source may occur, and enable more refined estimates of C emissions, thereby improving climate change forecasts.

Increases in area burned are largely attributed to an increased frequency of fires that burn over 10,000 ha; termed megafires (Stephens et al., 2014). It is generally expected that as area burned increases so will total C emissions (Bond-Lamberty et al., 2007; Turetsky et al., 2011). However, C emissions from boreal wildfires are strongly impacted by extensive spatial heterogeneity in ecological patterns and wildfire disturbance characteristics within individual fires. Therefore, fine-scale measurements do not contain all of the information needed to extrapolate to the total area burned and to estimate global-scale feedbacks (Peters & Herrick, 2004). A macroecological approach, that accounts for heterogeneities at one scale leading to nonlinear dynamics and the emergence of unpredictable patterns at other scales (Hamil, Huang, Fei, & Zhang, 2016; Heffernan et al., 2014; Peters, Bestelmeyer, & Turner, 2007), is required to estimate C emissions, determine the contribution of boreal wildfires to the global C cycle, and evaluate feedbacks to future climate.

The large areas covered by megafires have made it challenging to understand the major sources of heterogeneity in C emissions and thus accurately predict C emissions at macroscales. Emissions from wildfires are generally calculated as the product of mean fuel consumption, C concentrations per unit area, and the total burned area (Seiler & Crutzen, 1980). However, such direct extrapolations of plot-scale estimates of emissions (e.g., Mack et al., 2011) are likely to overestimate total emissions, due to biases of field measurements excluding low severity patches, unburned patches, and hydrological features (Hoy, Turetsky, & Kasischke, 2016; Veraverbeke, Rogers, & Randerson, 2015). Furthermore, plot-scale estimates of emissions are unlikely to be characteristic of macroscale emissions due to complex ecological patterns and spatial heterogeneity of fire severity associated with fuels, fire weather, and topography within fire perimeters (Falk, Miller, McKenzie, & Black, 2007; Peters et al., 2004; Turner, 2010). In particular, C emissions are impacted by both rapidly and slowly changing factors. Rapid dynamics that affect emissions include fire weather (Amiro, Stocks, Alexander, Flannigan, & Wotton, 2001; Barrett, Kasischke, McGuire, Turetsky, & Kane, 2010; de Groot, Pritchard, & Lynham, 2009) and seasonal changes in soil moisture (Turetsky et al., 2011). Emissions are also affected by slowly changing factors such as vegetation (de Groot et al., 2009), stand age (Brown & Johnstone, 2011; Hoy et al. 2016), and topographic features (Turetsky et al., 2011). Spatial heterogeneity in fuel loads and combustion can vary by roughly a factor of five at fine scales (Boby, Schuur, Mack, Verbyla, & Johnstone, 2010; Rogers et al., 2014) and are accordingly the largest source of uncertainty in emissions models. The spatial resolution of predictive models has varied from roughly 25 km in the case of a global model (van der Werf et al., 2017) to a 500 m regional model for Alaska and northwest Canada (Veraverbeke et al., 2017a). With increasing computing power and access to high-resolution remote sensed imagery, there is now an opportunity to provide emissions estimates at finer scales (e.g., 30 m pixels from Landsat imagery). Fine-scale estimates have the advantage of aligning better with the spatial resolution of ground plots, and provide a more accurate accounting of landscape heterogeneity.

The average area burned in boreal regions of Alaska and western Canada has substantially increased over recent decades (Gillett, Weaver, Zwiers, & Flannigan, 2004; Kasischke & Turetsky, 2006), and further increases by a factor of five are expected by the end of the century (Balshi et al., 2009; Boulanger, Gauthier, & Burton, 2014). In 2014, boreal megafires in the Northwest Territories (NWT), Canada burned a historically unprecedented 3.4 million hectares, more than eight times greater than the annual mean over the period of record (Canadian Interagency Forest Fire Center 2014). These megafires present a unique opportunity to assess the degree of spatial heterogeneity across a large fire complex, and whether the relative importance of fire weather, stand characteristics, and plot attributes on C emissions are different from past fire events, which were considerably smaller in spatial scale. Using a macrosystem approach we seek to identify the major sources of heterogeneity in C emissions of megafires and develop tools to extrapolate the emissions associated with such spatially extensive fire events.

Here, we develop a high spatial resolution model to scale emissions from the NWT megafires. We assessed both above- and below-ground C combustion in black spruce (*Picea mariana*) and jack pine (*Pinus banksiana*)-dominated forest stands, by far the most common type of forest burned. Our study design, data analysis, and extrapolation of emissions specifically account for spatial heterogeneity on the landscape by (i) randomly locating sites stratified by land cover or prefire tree species and time since last burn, in addition to (ii) systematically sampling plots of differing moisture regime within sites, (iii) using remote sensing imagery that aligns with the spatial scale of ground plots, and (iv) using hierarchical linear mixed effect models (Hamil et al., 2016). We expected that variables associated with plot-level attributes, fire characteristics, and stand composition, or some combination thereof, would impact combustion. As total C combustion (totalC) is not necessarily a complete metric of fire severity, we also assessed variations in total C combusted relative to total prefire carbon (propC), and the proportion of soil carbon combusted relative to total carbon combusted (propS). We hypothesized that:

1. totalC would be greatest in landscape positions of intermediate drainage, propC would decrease with increasing moisture, and

propS would increase with increasing moisture. This is because very dry sites have a shallow prefire soil organic layer (SOL) and are therefore likely to be completely combusted, whereas moist sites have a deep SOL, but the high moisture content is likely to prevent deep burning.

2. totalC, propC, and propS would increase with prefire stand age, as short fire return intervals do not allow sufficient time for the accumulation of SOL and result in less biomass available for severe burning.
3. totalC, propC, and propS would increase with late season burning and fire weather indices, as a result of the SOL drying out throughout the season and burning occurring when active layers have reached a maximum depth;
4. totalC, propC, and propS would increase with presence of black spruce and decrease with the presence of jack pine as black spruce stands have a thick, C-rich SOL available for combustion, whereas the majority of C in jack pine stands is stored aboveground in tree boles and is unavailable for combustion.

2 | MATERIALS AND METHODS

2.1 | Study area and site selection

This study took place near Yellowknife, Northwest Territories, Canada (Figure 1), where mean annual temperature was −4.3°C and mean annual precipitation was 290 mm from 1981 to 2010 (Environment Canada, 2015). The study area covers portions of two ecozones, the Taiga Plains and Taiga Shield, which differ in their geological history, soils development and parent materials (Ecosystem Classification Group, 2008, 2009). The Taiga Plains lie in an area of sedimentary geology while the Taiga Shield is dominated by exposed granite bedrock. Black spruce forests dominate the fine-textured, glacio-lacustrine soils found in both ecozones, while jack pine is dominant on the coarse, alluvial, and glacio-fluvial soils. Low-density black spruce and jack pine typically dominate the exposed bedrock characteristic of the Taiga Shield.

Between June and August of 2015, we conducted fieldwork in seven spatially independent burn scars, four in the Taiga Plains ecozone and three in the Taiga Shield ecozone, which had burned between June and August 2014 (Figure 1). See Supplementary Methods for details on the selection procedure of random sampling points. In the field, we located 3–12 random points ("A" plots) within each conifer density stratum or leading tree species (black spruce or jack pine) for each burn. We assessed moisture classes, based on topography-controlled drainage and adjusted for soil texture and presence of permafrost, for each random point on a six-point scale, ranging from xeric to subhygric, using the method outlined by Johnstone, Hollingsworth, and Chapin (2008). We then found at least one, but usually two, other points ("B" and "C" plots) that were of a different moisture class and within 100–500 m of the random point. We define a site as the combination of the random plot and these additional plots. We sampled a total of 211 burned plots nested within 78 randomly located sites. In June of 2016, we

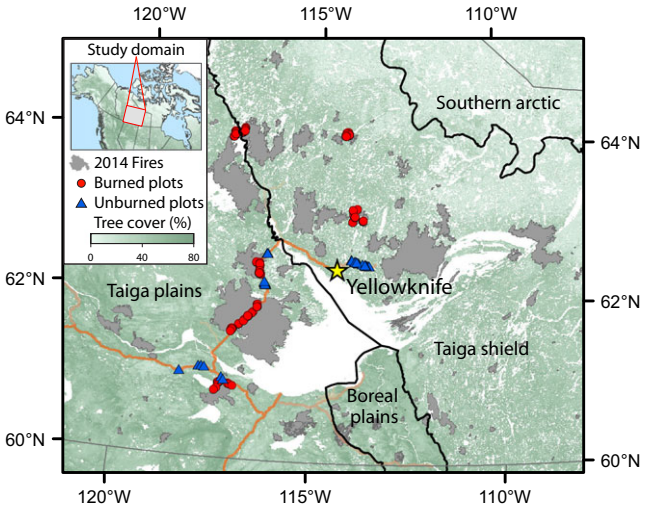

FIGURE 1 Map of the 2014 Northwest Territories fire complex showing locations of burned and unburned sampling plots. Bold black lines represent ecozone boundaries, light gray lines represent Provincial boundaries, and orange lines represent major roads

conducted field work in three spatially independent areas of forest, two in the Taiga Plains and one in the Taiga Shield (Figure 1), that had no history of fire since records began in the NWT in 1965. See Supplementary Methods for details on random selection procedure for 36 unburned plots.

2.2 | Field methods

At each plot we recorded latitude, longitude, and elevation with a GPS receiver, and slope and aspect with a clinometer and compass. Each plot consisted of two 30 m parallel transects that were 2 m apart. Transects ran due north.

Soil measurements were made along both transects within each plot. In burned and unburned stands, we measured SOL depth every 6 m (10 points/plot). To assess soil C, we collected the top 15 cm of the SOL profile in unburned plots or the entire residual SOL profile in burned plots at five points per plot along one transect. An intact sample of the SOL of approximately 5 cm × 10 cm was collected using a serrated knife and pruners. Dimensions of each SOL sample were recorded in the field. Organic samples were immediately frozen until they could be processed in the lab. In addition to the 10 SOL depth measurements, we also measured SOL depth near the base of ten trees per plot for burn depth calibrations. At these points, the SOL depth was measured as close to the tree as possible. In association with these points, we measured the depth from the top of the green moss to the closest adventitious root on one to three adventitious roots per tree in unburned stands, and the height from the highest adventitious root height (ARH) to the top of the residual SOL on one to three adventitious roots per tree in burned stands. These measurements were used for burn depth calibrations (see Figure S1 and Walker et al., 2018a).

In each plot, we measured the diameter at breast height (dbh) at the standard height of 1.3 m from the base, for all trees ≥1.3 m in

height and the basal diameter of trees <1.3 m tall that were originally rooted within a 2 m × 30 m belt transect. Fallen trees that were killed by fire were included in this census. We also assessed tree combustion, where each tree was ranked from 0 to 3; 0 = none, alive and no biomass combusted; 1 = low, only needles/leaves consumed; 2 = moderate, all foliage and majority of fine branches combusted; 3 = high, most of the aboveground canopy including foliage, branches, and bark combusted. To estimate stand age, we collected five basal tree discs in burned plots or five basal tree cores in unburned plots from each of the dominant tree species, either black spruce, jack pine, or both species.

2.3 | Laboratory methods

To assess soil bulk density and carbon (C) content in relation to depth, we obtained 1,025 soil monoliths from 211 burned plots in the summer of 2015 and 180 soil monoliths from 36 unburned plots in the summer of 2016. We processed (Figure S1) all monoliths from the 36 unburned plots and 350 monoliths from 134 burned plots. The subset of burned plots was chosen to encompass the full moisture gradient within all seven burns. In total, we analyzed 1,786 soil samples; 1,279 from burned sites and 507 from unburned sites. For subsequent analyses we excluded organic samples in which the carbon content was less than 20% as they likely contained mineral soil. This resulted in 507 samples from 137 monoliths collected in 36 unburned plots and 1,076 samples from 345 monoliths obtained from 134 burned plots.

Tree disks and cores were processed using standard dendrochronology techniques (Cook & Kairiukstis, 1990) and tree rings were counted as an estimate of time since last fire (see Walker et al., 2018a for details).

2.4 | Statistical analysis

All data analyses were performed using R statistical software version 3.4.3 (R Core Development Team, 2017). To test whether our access to sampling points introduced a bias in our field data, we used contingency table analysis with a Chi-square test to assess if the distribution of sampled plots (chosen in the field based on moisture regime) differed from the distribution across ecozones and moisture categories of our original randomly located points. A similar analysis was used to assess whether the distribution of sites among moisture categories differed between ecozones.

Stem counts, dbh, measurements, and published allometric equations (Lambert, Ung, & Raulier, 2005) were used to calculate tree density (number stems m^{-2}), basal area (m^2 ha^{-1}), and aboveground biomass (kg dry matter m^{-2}) of the total tree, bark, main branches, fine branches, and needles/leaves, for each tree species in each plot. Total tree biomass combusted was calculated per tree from the assigned combustion class and affected biomass components (foliage, branches, and bark). We summed individual tree estimates and divided by the sample area to estimate prefire biomass and biomass combustion (kg dry matter m^{-2}) per plot. We assumed a biomass C content of 50%.

To calculate depth of burn in black spruce-dominated stands we used the adventitious root method and calibrations described in Walker et al. (2018a), in which burn depth is equivalent to the height of adventitious roots (ARH) above the residual SOL plus an ARH offset associated with SOL depth (Figure S1). Total depth of prefire SOL was then reconstructed by adding the ARH and the associated offset to the residual SOL depth. In jack pine-dominated plots, where ARH measurements were not possible, we assessed depth of SOL combustion by subtracting the residual SOL from the unburned average SOL depth associated with each moisture category (see Walker et al., 2018a).

To model soil carbon content as a function of depth we used soil monoliths from unburned and burned plots. For each soil monolith (n = 534), we calculated the cumulative sums of carbon content by 5 cm depth increments (n = 1,518) starting from the surface, which was 0 cm in unburned plots, but was adjusted according to burn depth in burned plots. We used monoliths from both burned and unburned plots to ensure that the full range in SOL depths was captured. We fit linear mixed effects models with a hierarchical random effects structure of soil monolith nested within plot, nested within unburned area or burn scar, using the package "nlme" (Pinheiro et al., 2017). The response variable was log transformed to ensure normality. The depth covariate was accordingly log transformed to constrain the functional response. We fit separate models for black spruce (1,355 increments from 428 monoliths in 111 plots) and jack pine (163 increments from 106 soil monoliths in 30 plots)-dominated plots. The full models included covariates for depth, ecozone, and moisture category, and their first order interactions. Model reduction was completed through backward selection using likelihood ratio tests of the full model against the reduced models. For the minimum adequate model (Crawley, 2012) visual inspection of residual plots were examined for homoscedasticity and normality. Marginal R^2 (accounting only for fixed effects) and conditional R^2 values (accounting for random and fixed effects) were calculated using the "r.squaredGLMM" function in the package "MuMIn" (Barton & Barton, 2012) for this and all linear mixed effect models that follow.

We then used the models specific to each forest type to predict the carbon content (kg C m^{-2}) of both combusted (based on burn depth) and residual SOL for 10 measurements per plot. To test the accuracy of our models we compared the per monolith predicted residual carbon pools with measured residual carbon pools with a Student's t test. Prefire SOL carbon pools were calculated by summing the residual and the combusted carbon pools, which were then averaged per plot. For subsequent analysis we used the measured residual SOL carbon pool from the 134 plots for which direct measurements were made and the predicted SOL carbon pool from the remaining 77 plots.

We calculated three measures of carbon combustion for each plot (Table 1): (i) total carbon combusted (totalC) as the sum of above and belowground C combustion, (ii) proportion of prefire C combusted (propC) as totalC divided by the total prefire carbon, and (iii) proportional of totalC attributed to the soil organic layer (propS) as belowground C combustion divided by totalC. To assess which of

TABLE 1 Summary of measured plot characteristics and estimated carbon pools and combustion for 211 burned plots

Variable	Units	Mean ± *SD*	Range
Black spruce density	stems m^{-2}	0.62 ± 0.72	0.00–5.75
Black spruce basal area	m^2 ha^{-1}	7.19 ± 7.30	0.00–37.15
Jack pine density	stems m^{-2}	0.14 ± 0.45	0.00–4.85
Jack pine basal area	m^2 ha^{-1}	4.24 ± 6.92	0.00–28.93
Black spruce proportion	unitless	0.66 ± 0.24	0–1
Prefire aboveground tree biomass	kg dry matter m^{-2}	3.10 ± 2.64	0.004–18.14
Mean stand age	years	103 ± 45	19–232
Latitude	radians	1.09 ± 0.02	1.06–1.12
Moisture class	unitless	3.24 ± 1.76	1–6
Elevation	m.a.s.l.	265.0 ± 57.9	188.7–408.0
Slope	radians	0.03 ± 0.09	0–0.82
Aspect	radians	3.12 ± 1.73	0.00–6.16
Prefire organic layer depth	cm	22.9 ± 15.6	4.2–85.1
Burn depth	cm	8.6 ± 3.1	0.00–18.2
Prefire belowground carbon pool	kg C m^{-2}	11.0 ± 11.4	0.4–75.2
Prefire aboveground carbon pool	kg C m^{-2}	1.5 ± 1.3	1.8–9.1
Total prefire carbon pool (pre.totalC)	kg C m^{-2}	12.5 ± 11.3	1.1–75.3
Belowground carbon combusted (bC)	kg C m^{-2}	3.0 ± 1.9	0.3–9.1
Aboveground carbon combusted (aC)	kg C m^{-2}	0.4 ± 0.3	0–1.8
Total carbon combusted totalC = aC + bC	kg C m^{-2}	3.4 ± 2.0	0.3–9.3
Proportion of total prefire C combusted propC = totalC/pre.totalC	unitless	0.36 ± 0.22	0.04–0.92
Proportion of totalC from soil C combustion propS = bC/totalC	unitless	0.87 ± 0.12	0.30–1.00

Bolded variables are the three measures of carbon combustion we modeled.

our measured covariates were most closely related to totalC, propC, and propS, we initially examined six plot attributes, seven prefire stand composition variables, and six variables associated with fuel and weather conditions on the day of burning (Tables S1 and S2). To reduce collinearity, we derived a reduced set of covariates with no significant pairwise correlations (Spearman's $p < .05$) (Table 2). We defined a set of candidate models representative of our hypotheses regarding the factors affecting combustion (Table 2). Specifically, we hypothesized that combustion might be most affected by plot-level attributes, prefire stand composition, fire characteristics, or some combination of these factors. We scaled and centered all continuous covariates. The covariate for plot-level moisture category was included as a six-level factor using treatment contrasts, with "xeric" as the reference level. We log transformed total combustion to ensure normality. For each indicator and each candidate model, we fit a linear mixed effects model using the package "nlme" (Pinheiro et al., 2017), with random effects for site nested within burn to account for spatial dependencies. We calculated AIC_c (the sample size corrected Akaike information criterion) for each candidate model and ranked them by their Akaike weights using the R package "AICcmodavg" (Mazerolle & Mazerolle, 2017). We examined residual plots to test for heteroscedasticity and non-normality. We used model-averaged estimates over all candidate models to reduce model selection bias (Burnham & Anderson, 2002; Cade, 2015). We tested for differences in effect-sizes among moisture categories using Tukey–Kramer post hoc analysis for multiple comparisons in the R package "lsmeans" (Lenth, 2016). All data for the above analysis are available online (Walker et al., 2018b) and the R Code for the current analyses is provided in Supplementary Material.

2.5 | Spatial modeling

In order to spatially extrapolate our estimates of total combustion, we derived a similar model to that described above but using only covariates obtainable from geospatial layers that covered the entire spatial domain of interest. We initially considered 71 spatial layers associated with topography, permafrost condition, fire severity, tree cover, peatland cover, date of burn, fire weather, tree species biomass and percent cover, and soil properties (Table S2). Values for each plot were extracted using weighted averages of relevant pixels covering our 2 × 30 m transects. We removed explanatory variables that were significantly correlated with one another (Spearman's $p < .05$) within each predictor set. We then fit a multiple linear regression model to determine how total combustion (log transformed) was affected by the variables in each predictor set (Table S2). We retained the variables that were significant ($p < .05$) within each predictor set for inclusion in the final model. The final model predicted log of total combustion as a function of topographic wetness index, terrain ruggedness, differenced Normalized Burn Ratio (dNBR), relative change in tree cover, percent black spruce,

TABLE 2 Covariates included in each of the candidate models to predict total carbon combusted (totalC), total carbon combusted relative to total prefire carbon (propC), and the proportion of soil carbon combusted relative to total carbon combusted (propS)

Model	Variables
Null Model	None
M1: Plot-level attributes	Moisture class
	Elevation
	Stand age
	Latitude
M2: Prefire Stand Composition	Black spruce proportion
	Total above ground biomass
M3: Fire Attributes	Date of burn
	Fine Fuel Moisture Code
	Drought Moisture Code
M4: Plot-level attributes + Prefire Stand Composition	M1 + M2
M5: Plot-level attributes + Fire Attributes	M1 + M3
M6: Prefire Stand Composition + Fire Attributes	M2 + M3
Full Model	M1 + M2 + M3

and percent sand in the top 15 cm of soil. Model reduction was completed through backward stepwise selection using likelihood ratio tests of the full model against the reduced models. We examined residual plots to test for heteroscedasticity and non-normality, and conducted a 10-fold cross validation, repeated 100 times, to test against overfitting. For prediction purposes, the model's expected values were back-transformed from a log to a natural scale assuming a log-normal distribution (i.e., accounting for bias in the mean estimate), resulting in a multiplicative nonlinear regression model with similar structure to Veraverbeke et al. (2015).

We used this final model to estimate total C emissions at 30 m resolution across all fires in the 2014 NWT fire complex. Burned area was estimated based on past techniques using dNBR thresholds but adopted for our 30 m imagery and grid (see Supplementary Methods). Final model covariates were regridded to a common 30 m grid and Canadian Albers Equal Area Conic projection (nearest neighbor for datasets 30 m or finer and bilinear interpolation for data sets coarser than 30 m), defined by 28 tiles within the ABoVE (Arctic Boreal and Vulnerability Experiment) 30 m reference grid (Loboda, Hoy, & Carroll, 2017). For consistency, our regression model was rerun with these downscaled covariates. The regression model was then applied to all pixels that were defined as burned and had valid values for our final six covariates. To limit unreasonably high combustion estimates resulting from our nonlinear model, we applied a maximum cap on emissions, as in Rogers et al. (2014), of 1.2 times the maximum combustion observed at our field sites (9.26 kg C m^{-2}. Note this only applied to 0.02% of pixels). To provide an estimate of total emissions from the 2014 NWT complex, we scaled our estimate of total emissions to the complex considering the fraction of burned area not covered by our model (4%), assuming mean combustion in the missing burned pixels. To quantitate uncertainty, we adopted a Monte Carlo framework similar to Rogers et al. (2014) and Veraverbeke et al. (2015) that generated (i) mean pixel-level uncertainty, (ii) uncertainty in total emissions, and (iii) uncertainty in mean combustion (see Supplementary Methods for details). Uncertainty was assumed to arise from three major sources: measurement errors in aboveground and belowground combustion, and errors associated with landscape scaling arising from our geospatial layers and imperfect model fits (i.e., prediction uncertainty). All data for the spatial analysis are available online (Walker et al., 2018b) and the R Code is provided in Supplementary Material.

3 | RESULTS

3.1 | Stand characteristics

We assessed both aboveground and SOL carbon combustion in 211 burned forest plots, capturing a broad gradient in environmental characteristics and prefire stand composition (Table 1). Most plots were black spruce dominated (171 of 211), but many of these plots also had some jack pine trees present. Similarly, the 40 jack pine-dominated plots often had some black spruce trees present. We occasionally encountered other tree species such as white spruce (*Picea glauca*), balsam poplar (*Populus balsamifera*), paper birch (*Betula papyrifera*), trembling aspen (*Populus tremuloides*), and larch (*Larix laricina*), but these were always a small component of stand composition (maximum = 20% of stems).

The distribution of randomly located burned plots (A plots) did not differ from the distribution of the field-identified (B and C plots) across ecozones or moisture categories (X^2 = 11.578, df = 11, p = .396). Of the 211 burned plots we examined, 128 were located in the Taiga Plains and 83 were in the Taiga Shield ecozone. The distribution of these plots among moisture categories was significantly different between ecozones (X^2 = 13.196, df = 5, p = .02). On the Taiga Plains, plots were relatively evenly distributed among most moisture categories (17–31 plots in each category), aside from the subhygric category which had only eight plots. On the Taiga Shield, most plots were either classified as xeric (23 plots) or subhygric (20 plots), with the remainder being relatively evenly distributed (6–12 plots in each category).

3.2 | Pre- and postfire carbon pools and combustion

The final minimum adequate model of the cumulative sum of SOL carbon content (kg C m^{-2}) for black spruce plots included fixed effects of depth, ecozone, moisture, and all first-order interactions between these variables (marginal R^2 = .71, conditional R^2 = .92; Table S3). The minimum adequate model for jack pine plots included fixed effects of depth and moisture (marginal R^2 = .56, conditional R^2 = .66; Table S4). Using these models, the predicted residual SOL carbon pools were slightly higher than the measured pools (means of

6.61 vs. 6.07 kg C m^{-2}, respectively), but were not significantly different (Student's *t* test; $t = 0.936$, $df = 830.95$, $p = .349$).

The mean prefire carbon pool across all sites was 13.81 kg C m^{-2} with a range spanning two orders of magnitude from 0.5 to 86.67 kg C m^{-2}. The vast majority of this pool was from the SOL, with a mean of 11.95 kg C m^{-2} and a range of 0.31 to 86.52 kg C m^{-2} (Table 1). Mean total combustion across all sites was 3.35 kg C m^{-2} and ranged from 0.29 to 9.26 kg C m^{-2} (Table 1). Mean total combustion in black spruce-dominated stands was 3.90 kg C m^{-2} and ranged from 0.99 to 9.26 kg C m^{-2}. In jack pine-dominated stands, mean total carbon combustion was 0.70 kg C m^{-2} and ranged from 0.29 to 1.49 kg C m^{-2}. Of the mean total combustion, 90% or 3.00 kg C m^{-2} was attributed to SOL combustion.

Model selection indicated that variables associated with fuel conditions and weather at the time of fire were not important predictors of all three indicators of combustion. Of the tested hypotheses, the best model predicting totalC, propC, and propS was always M4, which included covariates for plot attributes and prefire stand composition (Table 2). The full model was equally as likely for predicting propS (Δ AICc <2; Table 3) and in all cases the only models with any probability (wi > 0) were M4 and the full model (Table 3). Moisture category was an important predictor of all three response variables, while latitude (which covaries with ecozone), elevation, and covariates associated with fire were not important (Table 4). totalC and propC also increased with the proportion of black spruce trees in the prefire stand and stand age (Table 4; Figures 2 and 3), and propC and propS decreased in association with increasing prefire tree biomass (Table 4; Figures 3 and 4).

3.3 | Spatial modeling

The final model used for spatial extrapolation of total combustion performed adequately, although not as well as our site-level models (adjusted $R^2 = .23$, overall $R^2 = .30$, and 10-fold cross validation $R^2 = .26$ for the logarithm of total combustion). This was despite relatively similar types of predictors (e.g., topographic wetness, terrain ruggedness, prefire species, and soil properties) as well as remotely sensed measures of fire severity (dNBR and relative change in tree cover). Nonetheless, this model resulted in substantial variability within and across fire perimeters (Figure 5). Mean combustion across all 2014 NWT fire pixels was 3.31 kg C m^{-2}, with a standard deviation of 1.14 kg C m^{-2}, and ranged from 0.59 to 11.12 kg C m^{-2}. Overall, the distribution of total combustion from the spatial model was similar to that measured at field plots (Table 1).

Our criteria for identifying burned pixels implied a total burned area of 2.85 Mha, substantially less than the total area of 3.57 Mha within official fire perimeters. The reduction in burned area resulted from accounting for small water bodies (reduction of 0.37 Mha) and applying our dNBR threshold identifying unburned pixels (reduction of 0.35 Mha or 11% of land area within fire

TABLE 3 Results of AICc-based model selection assessing the relationships between response variables of total carbon combusted (totalC), total carbon combusted relative to total prefire carbon (propC), and the proportion of soil carbon combusted relative to total carbon combusted (propS), to a set of linear mixed effect candidate models

		totalC						propC						propS					
Model	K	AICc	Δ AICc	wi	LogL	R_m	R_c	AICc	Δ AICc	wi	LogL	R_m	R_c	AICc	Δ AICc	wi	LogL	R_m	R_c
M4	**14**	**265.35**	**0**	**0.84**	**−117.52**	**0.67**	**0.67**	**−185.74**	**0**	**0.87**	**108.03**	**0.51**	**0.52**	**−427.63**	**0**	**0.68**	**228.97**	**0.62**	**0.67**
Full	17	268.69	3.34	0.16	−115.63	0.67	0.67	−182.01	3.73	0.13	109.72	0.52	0.52	**−426.1**	**1.53**	**0.32**	**231.76**	**0.63**	**0.66**
Null	4	440.12	174.77	0	−215.95	0	0.16	−80.44	105.31	0	44.32	0	0.11	−294.95	132.69	0	151.58	0	0.21
M1	12	308.14	42.8	0	−141.22	0.53	0.58	−152.46	33.28	0	89.08	0.39	0.44	−342.91	84.72	0	184.3	0.38	0.40
M2	6	310.85	45.5	0	−149.2	0.53	0.54	−76.54	109.21	0	45.56	0.00	0.10	−412.99	14.64	0	212.72	0.54	0.61
M3	7	439.08	173.73	0	−212.24	0.08	0.12	−150.66	35.08	0	91.66	0.05	0.07	−299.22	128.41	0	156.91	0.11	0.21
M5	15	309.11	43.76	0	−138.23	0.59	0.59	−72.95	112.79	0	45.96	0.42	0.44	−344.14	83.49	0	188.4	0.42	0.43
M6	9	314.96	49.61	0	−148	0.54	0.55	−76.95	108.8	0	44.7	0.07	0.08	−410.69	16.94	0	214.83	0.56	0.60

Variables included in each model are listed in Table 2. For each model the number of parameters (K), Log-likelihood, (LogL), the sample size corrected Akaike information criterion (AICc), the change in AICc relative to the best model (Δ AICc), the model weight (wi), the Log-likelihood, (LogL), the marginal R^2 (R_m—accounting for fixed effects only), and the conditional R^2 (R_c—accounting for both fixed and random effects) are given. Bold indicates the most probable model of those assessed based on AICc.

TABLE 4 Unbiased model-averaged parameter estimates for the nine factors considered in predicting total carbon combusted (totalC), total carbon combusted relative to total prefire carbon (propC), and the proportion of soil carbon combusted relative to total carbon combusted (propS)

Variables	totalC Estimate	totalC 95% CI	propC Estimate	propC 95% CI	propS Estimate	propS 95% CI
Intercept (Moisture class: Xeric)	**0.57**	**0.41 to 0.72**	**0.47**	**0.42 to 0.52**	**0.81**	**0.78 to 0.84**
Latitude (radians)	0.04	−0.05 to 0.12	0.03	0 to 0.06	0.01	0 to 0.02
Elevation (m.a.s.l.)	−0.02	−0.1 to 0.05	0.01	−0.02 to 0.03	0.02	−0.01 to 0.05
Stand age (years)	**0.13**	**0.06 to 0.20**	**0.03**	**0.01 to 0.05**	0.01	0 to 0.02
Black spruce proportion	**0.34**	**0.25 to 0.43**	**0.07**	**0.05 to 0.10**	0	−0.01 to 0.02
Total above ground biomass (kg dry matter m^{-2})	−0.02	−0.10 to 0.06	**−0.08**	**−0.08 to −0.03**	**−0.08**	**−0.09 to −0.06**
Date of Burn	−0.01	−0.06 to 0.04	0	−0.01 to 0.01	−0.01	−0.02 to 0.01
Fine Fuel Moisture Code	0	−0.03 to 0.04	0	−0.01 to 0.02	0	−0.01 to 0.02
Drought Moisture Code	−0.01	−0.06 to 0.04	0	−0.01 to 0.01	−0.01	−0.02 to 0.01
Moisture class						
Subxeric	**0.23**	**0.01 to 0.45**	0.05	−0.02 to 0.13	0.02	−0.02 to 0.06
Mesic–Subxeric	**0.60**	**0.37 to 0.83**	0	−0.08 to 0.07	**0.09**	**0.05 to 0.13**
Mesic	**0.71**	**0.47 to 0.95**	**−0.10**	**−0.18 to −0.03**	**0.09**	**0.05 to 0.13**
Mesic–Subhygric	**0.82**	**0.57 to 1.07**	**−0.26**	**−0.34 to −0.18**	**0.09**	**0.05 to 0.14**
Subhygric	**0.28**	**0.02 to 0.54**	**−0.40**	**−0.48 to −0.32**	**0.06**	**0.01 to 0.10**

Weights for model averaging are presented in Table 3. For each parameter the averaged model estimate (Estimate) and the 95% confidence intervals (CI) are provided. Bold represent important variables based on CI not including zero.

perimeters). Total emissions over all fire perimeters were estimated at 94.3 Tg C; 90.7 Tg C directly from the model and an added 3.5 Tg C when scaled by our estimate of 0.11 Mha burned area not captured due to missing satellite imagery. Our Monte Carlo simulations resulted in a mean pixel-level uncertainty of 2.2 kg C m^{-2}, with the largest contribution from prediction uncertainty in our model fits. Consistent with previous work (Rogers et al., 2014), these pixel-level prediction uncertainties tended to average out across the landscape, such that uncertainty in total domain-wide emissions was 7.9 Tg C, or 0.30 kg C m^{-2} for mean domain-wide combustion.

4 | DISCUSSION

The combustion estimates we present in this study indicate that total C combustion, the proportion of prefire C combusted, and the proportion attributed to the SOL were affected by slowly changing factors such as moisture class and the relative abundance of black spruce in the prefire stand, but not rapid dynamics associated with fire weather or date of burn. Our estimates of combustion suggest that black spruce stands located at landscape positions with intermediate drainage contribute the greatest to C emissions relative to other stands types and/or landscape positions. These variations in combustion associated with slowly changing factors elucidate the importance of using a macroscale approach to account for fine-scale heterogeneities in extrapolating C combustion to a larger spatial scale. Using these results, we estimated a total of 94.3 ± 7.9 Tg C emitted from 2.85 Mha of burned area across the entire 2014 NWT fire complex. These C emissions offset almost 50% of mean annual NEP in terrestrial ecosystems of Canada (197 Tg C $year^{-1}$ over the period 1990–2012; Chen, Hayes, & McGuire, 2017) and over ten times the mean annual NEP of boreal forest ecosystems of Alaska (8.3 Tg C $year^{-1}$ over the period 1950–2009; McGuire et al., 2018).

4.1 | Factors impacting C emissions

Our combustion metrics (totalC, propC, and propS) were all affected by slow changing factors and indicate that the greatest C combustion occurred in mature black spruce forests at intermediately drained landscape positions. As the vast majority (almost 90%) of total C combustion is from the SOL, this suggests that SOL available for combustion is largely limited by soil moisture, with near complete combustion at the driest landscape positions, to relatively low proportional combustion and the greatest proportion of combustion attributed to the SOL at the wettest areas on the landscape. These results support the hypothesized relationship that moisture and SOL depth control the potential for severe burning through smoldering combustion of the SOL and that the ecological effects of severe burning are likely to be greatest at sites of intermediate drainage (Johnstone & Chapin, 2006; Kane, Kasischke, Valentine, Turetsky, & McGuire, 2007).

Combustion associated with landscape positions is also confounded by prefire tree species combustion, where positions of intermediate drainage are often a mixture of jack pine and black spruce trees in this region. Accordingly, the greatest range in propC and propS occurred at the driest end of the gradient, which is likely due to the inclusion of jack pine-dominated plots, where a large portion of prefire C is stored aboveground in tree boles and is

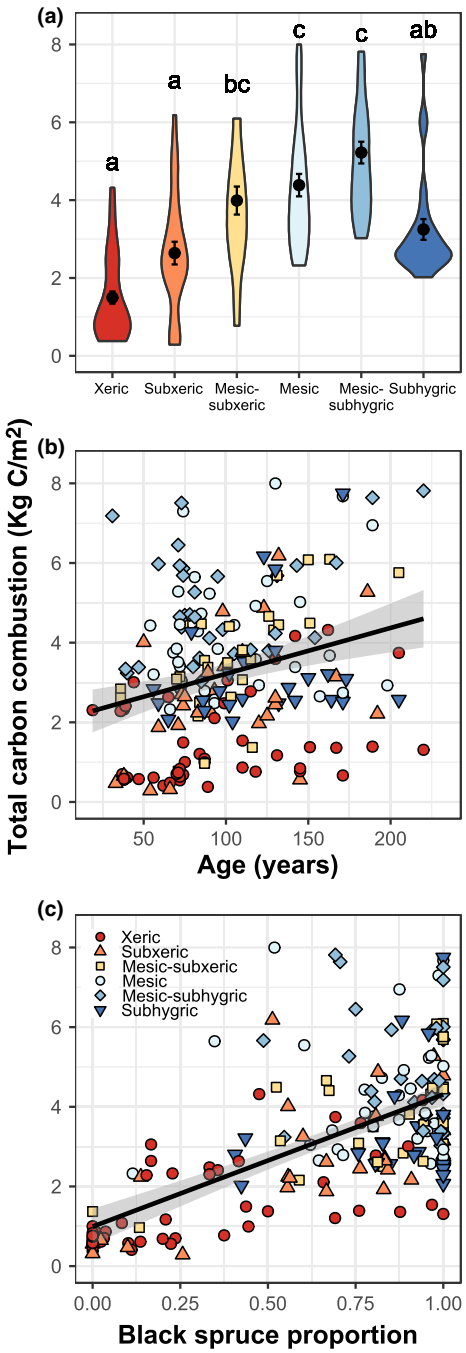

FIGURE 2 Total carbon combustion (totalC) as a function of (a) moisture category, (b) stand age, and (c) the proportion of black spruce stems relative to all stems in the plot. In (a) violin plots depict the data distribution, points and error bars represent the mean and standard error, and letters represent significant differences ($p < .05$) between moisture classes based on Tukey–Kramer post hoc test of multiple comparisons. Black lines in (b) and (c) represent simple linear regressions between the two variables with shading over the 95% confidence interval. See Table 4 for parameter estimates from fitted models and Figure S2 for plots of each model fitted covariate. See Figure S5 for plots of above and belowground C combusted as a function of age and black spruce proportion

unavailable for combustion. de Groot et al. (2009) also reported differences in emissions between jack pine and black spruce forests in this region, due to lower prefire SOL depths found in jack pine forests. The importance of prefire stand composition is also apparent by the decrease in both propC and propS in relation to prefire tree biomass, where increasing prefire tree biomass was generally an indication of jack pine presence.

Stand age in black spruce forests has also been shown to impact combustion and the proportion of the SOL that is combusted, with shorter fire return intervals resulting in lower postfire soil carbon stocks compared to a longer fire return interval (Brown & Johnstone, 2011; Hoy et al., 2016). In agreement, we found that as stand age increased, totalC and propC increased, but propS was not affected. As total prefire C, prefire SOL depth, and burn depth were all positively related to stand age and total C emissions (data not shown), this suggests that young stands, although contributing a relatively small amount to total C emissions, will have very little C remaining postfire and thus are more vulnerable to long-term changes in ecosystem C storage.

The Canadian Fire Weather Index (FWI) system (Stocks et al., 1998) has successfully been used to predict carbon emission in various fuel types throughout the boreal forest (Amiro et al., 2001; Barrett et al., 2010; de Groot et al., 2009), and date of burn has been shown to be one of the most important predictors of emission in black spruce forests in interior Alaska (Turetsky et al., 2011; Veraverbeke et al., 2015). We had, therefore, expected to see increased SOL combustion associated with late season burning, particularly for areas with deep organic layers, which is thought to be a result of the SOL drying out throughout the season and burning occurring when active layers have reached a maximum depth (Kasischke & Johnstone, 2005; Turetsky et al., 2011). The observed lack of relationship between combustion and date of burn in this study might therefore be due to the inclusion of jack pine plots, which have relatively little prefire SOL and no permafrost, and therefore would not dry out as much throughout the summer. However, we completed the same analyses examining black spruce and jack pine plots separately (data not shown) and in neither case was fire weather or date of burn important. Landscape position could also confound the relationship between combustion and date of burn. For example, mature black spruce forests in lowland positions within Alaska were unaffected by season of burn (Kane et al., 2007; Turetsky et al., 2011). However, we found no relationships between combustion and date of burn regardless of moisture classification (data not shown).

The most likely reason for not observing a relationship between combustion and date of burn or any FWIs is that all seven of the fires we examined burned within a relatively short period of time (July 2 to August 13), within one extreme fire season (2014), and within relatively close spatial proximity compared to past studies. Similarly, the lack of relationship between burn severity metrics and FWIs in the 2014 NWT fires was attributed

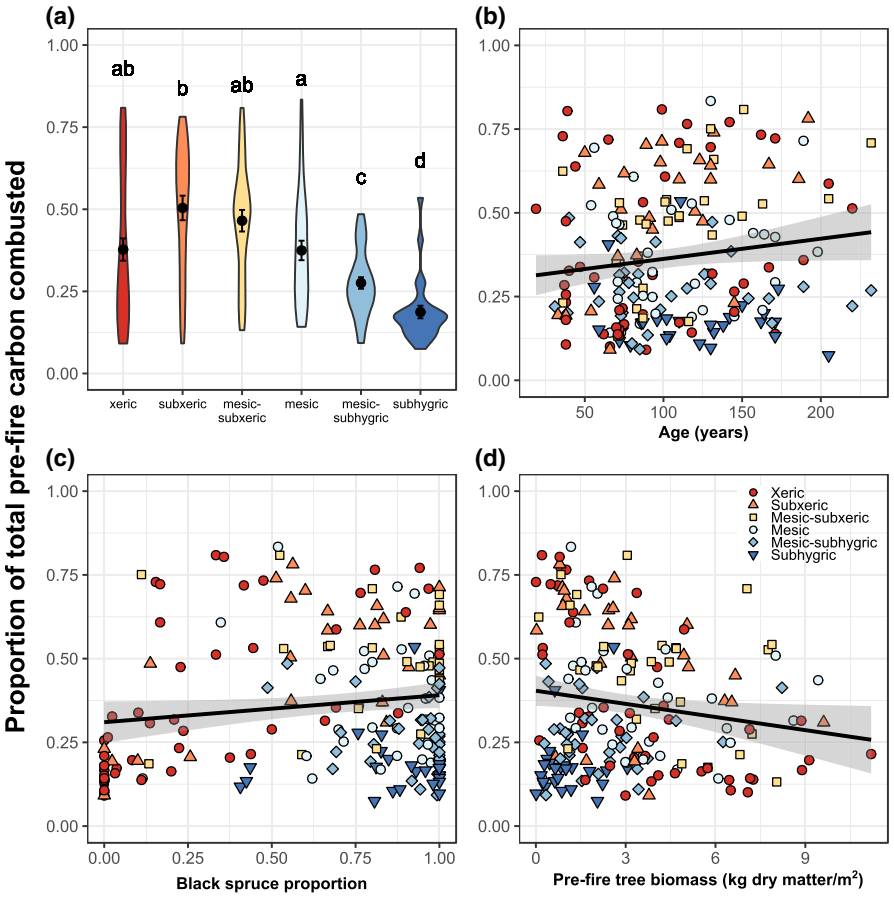

FIGURE 3 Proportion of total prefire carbon (propC) combusted as a function of (a) moisture category, (b) age, (c) the proportion of black spruce stems relative to all stems in the plot, and (d) prefire tree biomass. In (a) violin plots depict the data distribution, points and error bars represent the mean and standard error, and letters represent significant differences ($p < .05$) between moisture classes based on Tukey–Kramer post hoc test of multiple comparisons. Black lines in (b), (c), and (d) represent simple linear regressions between the two variables with shading over the 95% confidence interval. See Table 4 for parameter estimates and Figure S3 for plots of each model fitted covariate. See Figure S6 for plots of aboveground biomass prefire and aboveground biomass combusted as a function of black spruce proportion

to the very severe fire weather of 2014 resulting in low variability in FWIs (Whitman et al., 2018). In contrast, studies that included fires spanning a wider range in space and time conclude that day of burn (Turetsky et al., 2011; Veraverbeke et al., 2015) and FWIs (Amiro et al., 2001; Barrett et al., 2010; de Groot et al., 2009) are important predictors of emissions. Our assessment that C emissions were not affected by date of burn or FWIs with the 2014 NWT megafires suggests that variability in fire conditions may be confounded with spatial and temporal variability in other finer-scale or slow-moving factors.

4.2 | Comparison to other boreal wildfire emission estimates

Our mean combustion estimate of 3.35 kg C m^{-2}, which takes into account both black spruce and jack pine forest stands, is similar to other field-based estimates throughout the boreal forest in Alaska, but much higher than previous estimates in Canadian boreal forests (see Table 3 in Rogers et al., 2014). In jack pine-dominated stands, we found that mean total carbon combustion was 0.70 and 0.48 kg C m^{-2} was attributed to SOL combustion. Although field-based estimates of wildfire combustion in jack pine-dominated forests are rare, our results are within the range reported from experimental burns in Canadian jack pine forests of 0.5 kg C m^{-2} (0.4 kg C m^{-2} from soil) (Stocks et al., 1998) and 1.7 kg C m^{-2} from soil (de Groot et al., 2009). In black spruce-dominated plots, we found that mean carbon combustion was 3.88 and 3.51 kg C m^{-2} was attributed to soil organic layer burning. These results are within the range of combustion estimates reported for black spruce forest in interior of Alaska of 4.3 kg C m^{-2} (3.4 kg C m^{-2} from soil) (Kasischke et al., 2000) and 1.6 kg C m^{-2} (1.2 kg C m^{-2} from soil) (Neff, Harden, & Gleixner, 2005).

As combustion can vary significantly among fire scars and between years, we compared our combustion estimates to a similarly extreme fire year in 2004 in interior Alaska (Boby et al., 2010), which burned 2.4 million ha. Upon comparison, we found smaller burn depths yet greater combustion in the 2014 NWT fires. In our study, mean burn depth in black spruce-dominated stands was 9.4 cm (Walker et al., 2018a). In interior Alaska, a mean burn depth of 15.4 cm and combustion of 3.3, 2.9 kg C m^{-2} from soil, was reported (Boby et al., 2010). These differences are likely due to regional differences in surface bulk density. Samples from Alaska indicated a surface bulk density (green and brown moss) of 0.03 g cm^{-3} and bulk density of the fibric layer (approximate depth of 5 to 15 cm) was 0.05 g cm^{-3} (Boby et al., 2010). Although we did not divide our SOL samples into horizons, we found that bulk density of the top 5 cm was 0.07 g cm^{-3} and from 5 to 15 cm was 0.12 g cm^{-3}. These regional differences in bulk density, associated with soil development and the underlying parent material, explains the discrepancy between burn depth and combustion estimates between our study and previous studies from other regions in similarly extreme fire years.

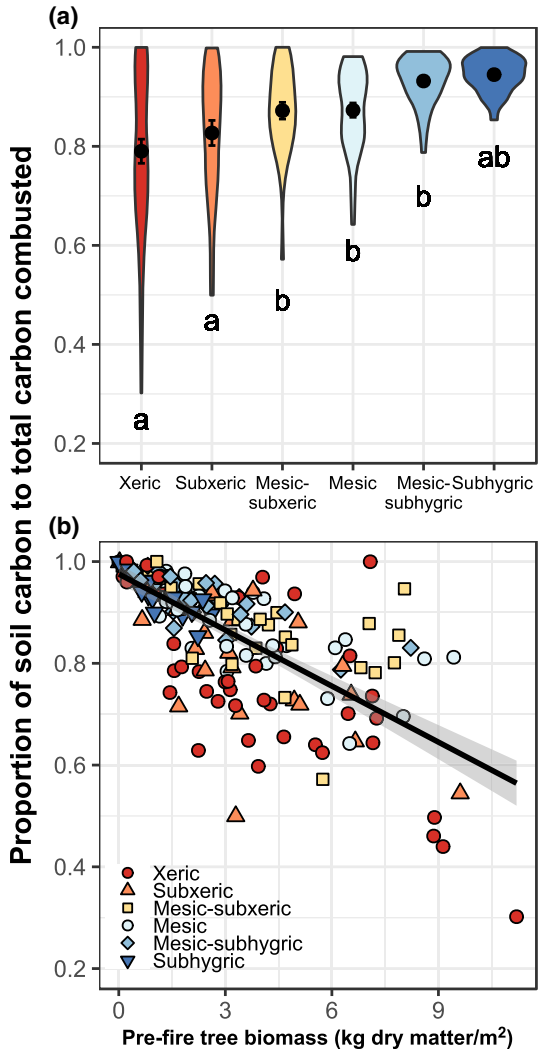

FIGURE 4 Proportion of carbon combustion attributed to the soil organic layer (propS) as a function of (a) moisture category, and (b) prefire tree biomass. In (a) violin plots depict the data distribution, points and error bars represent the mean and standard error, and letters represent significant differences ($p < .05$) between moisture classes based on Tukey–Kramer post hoc test of multiple comparisons. Black line in (b) represents a simple linear regression between the two variables with shading over the 95% confidence interval. See Table 4 for parameter estimates and Figure S4 for plots of each model fitted covariate

4.3 | Spatial modeling

The variance explained by our spatial model (overall $R^2 = .30$ and adjusted $R^2 = .23$ for the logarithm of total combustion) was comparable but slightly lower than previous efforts in Alaska. Veraverbeke et al. (2015) used a similar regression model trained on 126 black spruce plots in interior Alaska that spanned 21 fire complexes and five fire years, with an adjusted R^2 of .29 for belowground consumption and 0.53 for aboveground. Nevertheless, our model resulted in a median residual of 1.39 kg C m^{-2} for total combustion, which is similar to the sum of Veraverbeke et al. (2015)'s median residuals of 1.18 and 0.12 kg C m^{-2} for belowground and aboveground combustion, respectively. We hypothesize the slightly lower performance in our model was due to several factors: (i) as explained above, we sampled plots that spanned a narrower range in space and time, and (ii) in contrast to the marked topography of interior Alaska, small changes in elevation and landscape position in the NWT generate significant differences in site moisture, species, and prefire SOL layers. It may, therefore, be considerably more difficult for geospatial layers, such as DEM-derived topographic water indices, to capture these gradients. Moreover, our study design of three plots in close proximity with distinct moisture categories (i.e., one site) may have presented additional challenges for spatial modeling using geospatial layers with varying resolutions (Tables S2). Although we did not find FWIs to provide much predictive power, we note that our model performance is similar to de Groot et al. (2009) for soil consumption in wildfires ($R^2 \leq .25$), who built models based on FWIs and fires from multiple provinces and fire years. Finally, although machine learning has generated markedly higher R^2 values in Alaska (Barrett, McGuire, Hoy, & Kasischke, 2011; Barrett et al., 2010), this modeling technique has been shown to overfit when using only roughly 100–200 observations, and is therefore less suited for extrapolation (Veraverbeke et al., 2015).

Our estimated burned area for the 2014 NWT fires (2.85 Mha) was less than several previous estimates using coarser-scale MODIS imagery, including a similar regional approach (3.41 Mha, Veraverbeke et al., 2017b) and the Global Fire Emissions Database (GFED, 3.11 Mha, van der Werf et al., 2017). Our estimate is corroborated by Canada's National Burned Area Composite (NBAC, de Groot et al., 2007), which reported 2.81 Mha of burned area in 2014 NWT fires. NBAC employs a multisensor approach to map most fires since 2004 at a relatively high level of detail. We attribute the differences to spatial scaling properties associated with small water bodies in the NWT, many of which are smaller than a 500 m pixel (see example in Figure 5). As these inland water bodies are extensive across much of the region (Carroll, Wooten, DiMiceli, Sohlberg, & Kelly, 2016; Feng, Sexton, Channan, & Townshend, 2016), especially the Shield ecozone, we suggest burned area estimates derived from moderate to coarse-scale imagery should be adjusted for the inclusion of water bodies. In addition to neglecting small water bodies, the Provincial/National fire perimeters include many unburned areas within fire scars, resulting in a high estimate of total burned area (3.57 Mha). Users should be aware of these issues when using the Canadian (and Alaskan) National Fire Databases to analyze burned area dynamics in North America's boreal forests.

Uncertainties in burned area influence estimates of total C emissions. For example, Veraverbeke et al. (2017b) estimated that the 2014 NWT fires emitted 164 ± 32 Tg C. This is 74% higher than our estimate (94.3 ± 7.9 Tg C), a result of both higher burned area and mean combustion (4.81 ± 0.94 kg C m^{-2} vs. our estimate of 3.31 ± 0.30 kg C m^{-2}). Regarding the latter, it should be noted that Veraverbeke et al. (2017b) trained their model on black spruce plots in Alaska. Our study, therefore, adds to the argument that the

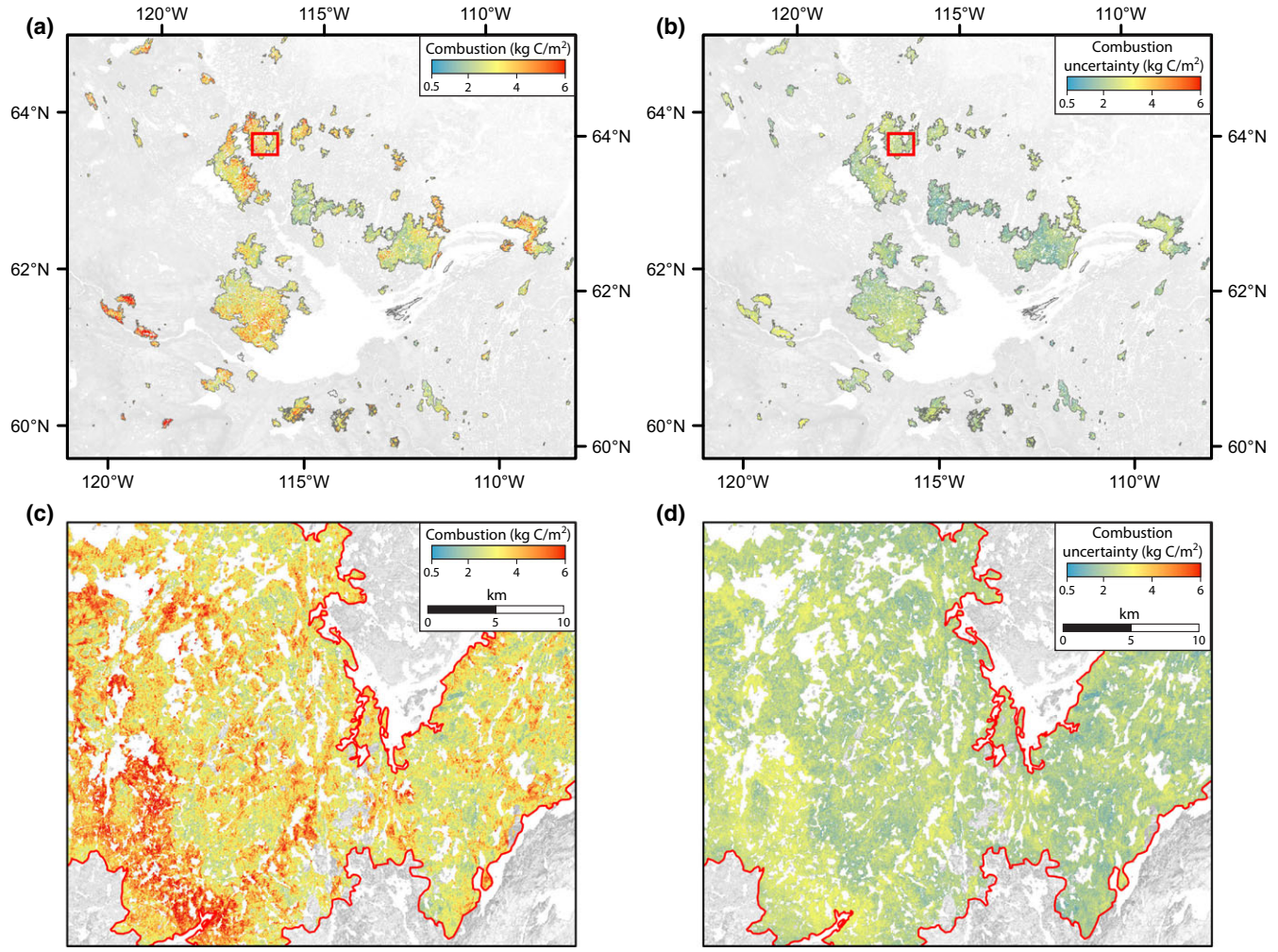

FIGURE 5 Maps of the 2014 NWT fire complex showing (a) estimated total combustion, (b) uncertainty in total combustion, and details of landscape heterogeneity in (c) combustion and (d) uncertainty within one of the major fire scars. The maps are focused on the major fire perimeters, although our spatial model includes some perimeters not shown (5% of total burned area). The extent of panels (c) and (d) are shown as red boxes in panels (a) and (b)

relationships between geospatial variables and ecosystem properties that influence combustion differ significantly between regions in the boreal forest, and can be accounted for by incorporating representative field observations. We also note that despite estimating slightly more burned area, the GFED model estimated a similar amount of total C emissions from the 2014 NWT fires (86.8 Tg C) due to slightly lower mean combustion (2.79 kg C m^{-2}).

A caveat with these comparisons is that our pixel-level uncertainty was high (2.2 kg C m^{-2} or 66% of the mean). This was almost entirely due to prediction error in our model fits. Because site moisture and prefire tree species were the most important site-level predictors, we suggest that improved spatial layers related to these properties would significantly improve regional models of combustion, both in the NWT and throughout the boreal biome. Nonetheless, the distribution of domain-wide combustion values from our spatial model was similar to that from field observations, albeit with smaller variability. Uncertainties in estimated total emissions (7.9 Tg C) and mean domain-wide combustion (0.30 kg C m^{-2}) were also considerably smaller than uncertainty at the pixel level. This supports the use of our statistical model in the region, understanding that combustion estimates at the landscape scale will be more robust than at any one particular pixel or site. It also speaks to the representativeness of our field sampling. Overall, our results provide support for developing 30 m fire C emissions estimates across large domains in the boreal forest by integrating representative field observations. Presumably, integrating sites from a wider array of regions, environmental conditions, and fire years can improve these models.

4.4 | Implications

In response to climate change the size, severity, and frequency of boreal forest fires has been increasing, a trend that is expected to continue. Such changes have the potential to alter the net ecosystem C balance (Harden et al., 2000), catalyze shifts in postfire successional trajectories (Johnstone & Chapin, 2006; Johnstone,

Hollingsworth, Chapin, & Mack, 2010), promote permafrost degradation (Nossov, Jorgenson, Kielland, & Kanevskiy, 2013; Shur & Jorgenson, 2007), change soil moisture regimes (Schuur et al., 2008), and decrease soil microbial biomass and respiration (Holden, Gutierrez, & Treseder, 2013). The unprecedentedly large area that burned in the NWT in 2014 may become more common as the climate continues to warm and dry. Using a macroecological approach of randomly locating sites, systematically sampling plots of different moisture classes, and analyzing data with hierarchical linear mixed models to account for fine-scale heterogeneities, we identified the major sources of variation in C emissions and found that black spruce forests in landscape positions of intermediate drainage are most vulnerable to changes in C in both the Taiga Plains and Taiga Shield ecozones. Furthermore, as fire frequency increases and immature stands burn, the total C storage in both aboveground and belowground biomass will likely decrease. Increased combustion associated with an intensifying fire regime could shift boreal ecosystems from net accumulation of C from the atmosphere over multiple fire cycles, to a net loss. In order for this shift to occur, fires would have to release old carbon that escaped combustion in one or more previous fires. Future research which examines the relationship between burn depth, combustion, and the release of old C could provide insight into whether or not this shift has or could occur in boreal forest ecosystems after an extreme fire year. Our results highlight the need for regionally specific calibrations that account for spatial heterogeneity in order to accurately model emissions at a continental scale. Our models and spatial extrapolation should also allow future research to model emissions over larger temporal and spatial scales, including the under-represented areas of the Taiga Plains and Taiga Shield. Accurately estimating C emissions from fires is critical for assessing the implications of changes in the fire regime on successional trajectories, permafrost dynamics, carbon stocks, and their associated feedbacks to longer term C storage and climate.

ACKNOWLEDGEMENTS

This project was supported by funding awarded to MCM from NSF DEB RAPID grant #1542150, and from the NASA Arctic Boreal and Vulnerability Experiment (ABoVE) Legacy Carbon grant: #Mack-01; NSERC Discovery Grant funding to JFJ and MRT; Government of the Northwest Territories Cumulative Impacts Monitoring Program Funding project #170 to JLB; and Polar Knowledge Canada's Northern Science Training Program funding awarded to Canadian field assistants. We thank our lab members at Northern Arizona University for their input and feedback at various stages of this manuscript. We extend our appreciation to the numerous field and laboratory assistants and graduate students from Northern Arizona University, Wilfrid Laurier University, and University of Guelph. We also thank David McGuire and Dan Hayes for help with Alaska and Canada-wide NEP estimates. We are grateful for the support provided by the Government of the Northwest Territories – Wilfrid Laurier University Partnership Agreement for important logistical support and access to lab space.

ORCID

Xanthe J. Walker http://orcid.org/0000-0002-2448-691X
Brendan M. Rogers http://orcid.org/0000-0001-6711-8466
Nicola J. Day http://orcid.org/0000-0002-3135-7585
Scott J. Goetz http://orcid.org/0000-0002-6326-4308

REFERENCES

Amiro, B. D., Stocks, B. J., Alexander, M. E., Flannigan, M. D., & Wotton, B. M. (2001). Fire, climate change, carbon and fuel management in the Canadian boreal forest. *International Journal of Wildland Fire*, *10*, 405. https://doi.org/10.1071/WF01038

Balshi, M. S., McGuire, A., Duffy, P., Flannigan, M., Walsh, J., & Melillo, J. (2009). Assessing the response of area burned to changing climate in western boreal North America using a Multivariate Adaptive Regression Splines (MARS) approach. *Global Change Biology*, *15*, 578–600. https://doi.org/10.1111/j.1365-2486.2008.01679.x

Barrett, K., Kasischke, E. S., McGuire, A. D., Turetsky, M. R., & Kane, E. S. (2010). Modeling fire severity in black spruce stands in the Alaskan boreal forest using spectral and non-spectral geospatial data. *Remote Sensing of Environment*, *114*, 1494–1503. https://doi.org/10.1016/j.rse.2010.02.001

Barrett, K., McGuire, A. D., Hoy, E. E., & Kasischke, E. S. (2011). Potential shifts in dominant forest cover in interior Alaska driven by variations in fire severity. *Ecological Applications*, *21*, 2380–2396. https://doi.org/10.1890/10-0896.1

Barton, K., & Barton, M. K. (2012). Package 'MuMIn': model selection and model average based on information criteria (AICc and alike). CRAN R Project.

Boby, L. A., Schuur, E. A., Mack, M. C., Verbyla, D., & Johnstone, J. F. (2010). Quantifying fire severity, carbon, and nitrogen emissions in Alaska's boreal forest. *Ecological Applications*, *20*, 1633–1647. https://doi.org/10.1890/08-2295.1

Bond-Lamberty, B., Peckham, S. D., Ahl, D. E., & Gower, S. T. (2007). Fire as the dominant driver of central Canadian boreal forest carbon balance. *Nature*, *450*, 89–92. https://doi.org/10.1038/nature06272

Boulanger, Y., Gauthier, S., & Burton, P. J. (2014). A refinement of models projecting future Canadian fire regimes using homogeneous fire regime zones. *Canadian Journal of Forest Research*, *44*, 365–376. https://doi.org/10.1139/cjfr-2013-0372

Bradshaw, C. J. A., & Warkentin, I. G. (2015). Global estimates of boreal forest carbon stocks and flux. *Global and Planetary Change*, *128*, 24–30. https://doi.org/10.1016/j.gloplacha.2015.02.004

Brown, C. D., & Johnstone, J. F. (2011). How does increased fire frequency affect carbon loss from fire? A case study in the northern boreal forest. *International Journal of Wildland Fire*, *20*, 829–837. https://doi.org/10.1071/WF10113

Burnham, K. P., & Anderson, D. R. (2002). *Model selection and multimodel inference: A practical information-theoretic approach*, 2nd edn. Springer-Verlag, New York, NY.

Cade, B. S. (2015). Model averaging and muddled multimodel inferences. *Ecology*, *96*, 2370–2382. https://doi.org/10.1890/14-1639.1

Canadian Interagency Forest Fire Center. (2014). Situation Report – Sep 22, 2014. Available at http://www.ciffc.ca/firewire/current.php?lang=en&date=20140922. Accessed 21 December 2017.

Carroll, M., Wooten, M., DiMiceli, C., Sohlberg, R., & Kelly, M. (2016). Quantifying surface water dynamics at 30 meter spatial resolution in the North American High Northern Latitudes 1991-2011. *Remote Sensing*, *8*, 622. https://doi.org/10.3390/rs8080622

Chen, G., Hayes, D. J., & McGuire, A. D. (2017). Contributions of wildland fire to terrestrial ecosystem carbon dynamics in North America

from 1990 to 2012. *Global Biogeochemical Cycles*, *31*, 878–900. https://doi.org/10.1002/2016GB005548

Cook, E. R., & Kairiukstis, L. (1990). *Methods of dendrochronology: Applications in the Environmental Sciences*. Kluwer Academic Publishers, Dordrecht, the Netherlands.

Commane, R., Lindaas, J., Benmergui, J., Luus, K. A., Chang, R. Y., Daube, B. C., … Wofsy, S. C. (2017). Carbon dioxide sources from Alaska driven by increasing early winter respiration from Arctic tundra. *Proceedings of the National Academy of Sciences*, *114*, 5361–5366. https://doi.org/10.1073/pnas.1618567114

Crawley, M. J. (2012). *The R book*, 2nd ed. Oxford: Wiley. https://doi.org/10.1002/9781118448908

de Groot, W. J., Landry, R., Kurz, W. A., Anderson, K. R., Englefield, P., Fraser, R. H., … Pritchard, J. (2007). Estimating direct carbon emissions from Canadian wildland fires. *International Journal of Wildland Fire*, *16*, 593–606. https://doi.org/10.1071/WF06150

de Groot, W. J., Pritchard, J. M., & Lynham, T. J. (2009). Forest floor fuel consumption and carbon emissions in Canadian boreal forest fires. *Canadian Journal of Forest Research*, *39*, 367–382. https://doi.org/10.1139/X08-192

Ecosystem Classification Group. (2008). *Ecological regions of the northwest territories – Taiga Shield*. Yellowknife: Department of Environment and Natural Resources, Government of the Northwest Territories.

Ecosystem Classification Group. (2009). *Ecological regions of the northwest territories – Taiga Plains*. Yellowknife: Department of Environment and Natural Resources, Government of the Northwest Territories.

Environment Canada. (2015). Station records for Yellowknife, NWT, Canada. Available at http://climate.weather.gc.ca/climate_normals/index_e.html. Accessed 1 February 2019.

Falk, D. A., Miller, C., McKenzie, D., & Black, A. E. (2007). Cross-scale analysis of fire regimes. *Ecosystems*, *10*, 809–823. https://doi.org/10.1007/s10021-007-9070-7

Feng, M., Sexton, J. O., Channan, S., & Townshend, J. R. (2016). A global, high-resolution (30-m) inland water body dataset for 2000: First results of a topographic-spectral classification algorithm. *International Journal of Digital Earth*, *9*, 113–133. https://doi.org/10.1080/17538947.2015.1026420

Gillett, N. P., Weaver, A. J., Zwiers, F. W., & Flannigan, M. D. (2004). Detecting the effect of climate change on Canadian forest fires. *Geophysical Research Letters*, *31*, L18211. https://doi.org/10.1029/2004GL020876

Hamil, K. A. D., Huang, W. K., Fei, S., & Zhang, H. (2016). Cross-scale contradictions in ecological relationships. *Landscape Ecology*, *31*, 7–18. https://doi.org/10.1007/s10980-015-0288-z

Harden, J. W., Trumbore, S. E., Stocks, B. J., Hirsch, A., Gower, S. T., O'neill, K. P., & Kasischke, E. S. (2000). The role of fire in the boreal carbon budget. *Global Change Biology*, *6*, 174–184. https://doi.org/10.1046/j.1365-2486.2000.06019.x

Heffernan, J. B., Soranno, P. A., Angilletta, M. J., Buckley, L. B., Gruner, D. S., Keitt, T. H., … Weathers, K. C. (2014). Macrosystems ecology: Understanding ecological patterns and processes at continental scales. *Frontiers in Ecology and the Environment*, *12*, 5–14. https://doi.org/10.1890/130017

Holden, S. R., Gutierrez, A., & Treseder, K. K. (2013). Changes in soil fungal communities, extracellular enzyme activities, and litter decomposition across a fire chronosequence in Alaskan boreal forests. *Ecosystems*, *16*, 34–46. https://doi.org/10.1007/s10021-012-9594-3

Hoy, E. E., Turetsky, M. R., & Kasischke, E. S. (2016). More frequent burning increases vulnerability of Alaskan boreal black spruce forests. *Environmental Research Letters*, *11*, 095001. https://doi.org/10.1088/1748-9326/11/9/095001

Johnstone, J., & Chapin, F. (2006). Effects of soil burn severity on post-fire tree recruitment in boreal forest. *Ecosystems*, *9*, 14–31. https://doi.org/10.1007/s10021-004-0042-x

Johnstone, J. F., Hollingsworth, T. N., & Chapin, F. S. (2008). A key for predicting postfire successional trajectories in black spruce stands of interior Alaska. General Technical Report—Pacific Northwest Research Station, USDA Forest Service, i + 37 pp.

Johnstone, J. F., Hollingsworth, T. N., Chapin, F. S., & Mack, M. C. (2010). Changes in fire regime break the legacy lock on successional trajectories in Alaskan boreal forest. *Global Change Biology*, *16*, 1281–1295. https://doi.org/10.1111/j.1365-2486.2009.02051.x

Kane, E. S., Kasischke, E. S., Valentine, D. W., Turetsky, M. R., & McGuire, A. D. (2007). Topographic influences on wildfire consumption of soil organic carbon in interior Alaska: Implications for black carbon accumulation. *Journal of Geophysical Research: Biogeosciences*, *112*, G03017.

Kasischke, E. S., French, N. H. F., O'Neill, K. P., Richter, D. D., Bourgeau-Chavez, L. L., Harell, P. A., & Stocks, B. J. (2000). Influence of fire on long-term patterns of forest succession in Alaskan boreal forests. In *Ecological Studies; Fire, climate change, and carbon cycling in the Boreal Forest*, pp. 214–238. https://doi.org/10.1007/978-0-387-21629-4

Kasischke, E. S., & Johnstone, J. F. (2005). Variation in postfire organic layer thickness in a black spruce forest complex in interior Alaska and its effects on soil temperature and moisture. *Canadian Journal of Forest Research*, *35*, 2164–2177. https://doi.org/10.1139/x05-159

Kasischke, E. S., & Turetsky, M. R. (2006). Recent changes in the fire regime across the North American boreal region—Spatial and temporal patterns of burning across Canada and Alaska. *Geophysical Research Letters*, *33*, L09703.

Kasischke, E. S., Verbyla, D. L., Rupp, T. S., McGuire, A. D., Murphy, K., Jandt, R., … Turetsky, M. R. (2010). Alaska's changing fire regime—implications for the vulnerability of its boreal forests. *Canadian Journal of Forest Research*, *40*, 1313–1324. https://doi.org/10.1139/X10-098

Lambert, M.-C., Ung, C.-H., & Raulier, F. (2005). Canadian national tree aboveground biomass equations. *Canadian Journal of Forest Research*, *35*, 1996–2018. https://doi.org/10.1139/x05-112

Lenth, R. V. (2016). Least-squares means: The R package lsmeans. *Journal of Statistical Software*, *69*, 1–33.

Li, F., Lawrence, D. M., & Bond-Lamberty, B. (2017). Impact of fire on global land surface air temperature and energy budget for the 20th century due to changes within ecosystems. *Environmental Research Letters*, *12*, 044014. https://doi.org/10.1088/1748-9326/aa6685

Loboda, T. V., Hoy, E. E., & Carroll, M. L. (2017). ABoVE: Study Domain and Standard Reference Grids.

Mack, M. C., Bret-Harte, M. S., Hollingsworth, T. N., Jandt, R. R., Schuur, E. A. G., Shaver, G. R., & Verbyla, D. L. (2011). Carbon loss from an unprecedented Arctic tundra wildfire. *Nature*, *475*, 489–492. https://doi.org/10.1038/nature10283

Mazerolle, M. J., & Mazerolle, M. M. J. (2017). Package "AICcmodavg." AICcmodavg: model selection and multimodel inference based on (Q) AIC (c) CRAN R Project.

McGuire, D., Genet, H., Lyu, A., Pastick, N., Stackpoole, S., Birdsey, R., … Zhu, Z. (2018). Assessing historical and projected carbon balance of Alaska: A synthesis of results and policy/management implications. *Ecological Applications*.

Neff, J. C., Harden, J. W., & Gleixner, G. (2005). Fire effects on soil organic matter content, composition, and nutrients in boreal interior Alaska. *Canadian Journal of Forest Research*, *35*, 2178–2187. https://doi.org/10.1139/x05-154

Nossov, D. R., Jorgenson, M. T., Kielland, K., & Kanevskiy, M. Z. (2013). Edaphic and microclimatic controls over permafrost response to fire in interior Alaska. *Environmental Research Letters*, *8*, 035013. https://doi.org/10.1088/1748-9326/8/3/035013

Pan, Y., Birdsey, R. A., Fang, J., Houghton, R., Kauppi, P. E., Kurz, W. A., … Hayes, D. (2011). A large and persistent carbon sink in the World's Forests. *Science*, *333*, 988–993. https://doi.org/10.1126/science.1201609

Peters, D. P. C., Bestelmeyer, B. T., & Turner, M. G. (2007). Cross-scale interactions and changing pattern-process relationships: Consequences for system dynamics. *Ecosystems*, *10*, 790–796. https://doi.org/10.1007/s10021-007-9055-6

Peters, D. P. C., & Herrick, J. E. (2004). Strategies for ecological extrapolation. *Oikos*, *106*, 627–636. https://doi.org/10.1111/j.0030-1299.2004.12869.x

Peters, D. P. C., Pielke, R. A., Bestelmeyer, B. T., Allen, C. D., Munson-McGee, S., & Havstad, K. M. (2004). Cross-scale interactions, nonlinearities, and forecasting catastrophic events. *Proceedings of the National Academy of Sciences of the United States of America*, *101*, 15130–15135. https://doi.org/10.1073/pnas.0403822101

Pinheiro, J., Bates, D., DebRoy, S., Sarkar, D., Heisterkamp, S., Van Willigen, B., & Maintainer, R. (2017). Package "nlme." *Linear and Nonlinear Mixed Effects Models*, *version*, 3–1. CRAN R Project.

R Core Development Team. (2017). *R: A language and environment for statistical computing v. 3.4.3*. Vienna: R Foundation for Statistical Computing.

Randerson, J. T., Liu, H., Flanner, M. G., Chambers, S. D., Jin, Y., Hess, P. G., … Zender, C. S. (2006). The impact of boreal forest fire on climate warming. *Science*, *314*, 1130–1132. https://doi.org/10.1126/science.1132075

Rogers, B. M., Veraverbeke, S., Azzari, G., Czimczik, C. I., Holden, S. R., Mouteva, G. O., … Randerson, J. T. (2014). Quantifying fire-wide carbon emissions in interior Alaska using field measurements and Landsat imagery. *Journal of Geophysical Research: Biogeosciences*, *119*, 1608–1629.

Schuur, E. A., Bockheim, J., Canadell, J. G., Euskirchen, E., Field, C. B., Goryachkin, S. V., … Zimov, S. A. (2008). Vulnerability of permafrost carbon to climate change: Implications for the global carbon cycle. *BioScience*, *58*, 701–714. https://doi.org/10.1641/B580807

Seiler, W., & Crutzen, P. J. (1980). Estimates of gross and net fluxes of carbon between the biosphere and the atmosphere from biomass burning. *Climatic Change*, *2*, 207–247. https://doi.org/10.1007/BF00137988

Shur, Y. L., & Jorgenson, M. T. (2007). Patterns of permafrost formation and degradation in relation to climate and ecosystems. *Permafrost and Periglacial Processes*, *18*, 7–19. https://doi.org/10.1002/(ISSN)1099-1530

Stephens, S. L., Burrows, N., Buyantuyev, A., Gray, R. W., Keane, R. E., Kubian, R., … Tolhurst, K. G. (2014). Temperate and boreal forest mega-fires: Characteristics and challenges. *Frontiers in Ecology and the Environment*, *12*(115–122), 115–122. https://doi.org/10.1890/120332

Stocks, B. J., Fosberg, M. A., Lynham, T. J., Mearns, L., Wotton, B., Yang, Q., … Mckenney, D. (1998). Climate change and forest fire potential in Russian and Canadian boreal forests. *Climatic Change*, *38*, 1–13. https://doi.org/10.1023/A:1005306001055

Turetsky, M. R., Kane, E. S., Harden, J. W., Ottmar, R. D., Manies, K. L., Hoy, E., & Kasischke, E. S. (2011). Recent acceleration of biomass burning and carbon losses in Alaskan forests and peatlands. *Nature Geoscience*, *4*, 27–31. https://doi.org/10.1038/ngeo1027

Turner, M. G. (2010). Disturbance and landscape dynamics in a changing world 1. *Ecology*, *91*, 2833–2849. https://doi.org/10.1890/10-0097.1

van der Werf, G. R., Randerson, J. T., Giglio, L., van Leeuwen, T. T., Chen, Y., Rogers, B. M., … Kasibhatla, P. S. (2017). Global fire emissions estimates during 1997–2016. *Earth System Science Data*, *9*, 697–720. https://doi.org/10.5194/essd-9-697-2017

Veraverbeke, S., Rogers, B. M., Goulden, M. L., Jandt, R., Miller, C. E., Wiggins, E. B., & Randerson, J. T. (2017a). ABoVE: Ignitions, burned area and emissions of fires in AK, YT, and NWT, 2001-2015.

Veraverbeke, S., Rogers, B. M., Goulden, M. L., Jandt, R. R., Miller, C. E., Wiggins, E. B., & Randerson, J. T. (2017b). Lightning as a major driver of recent large fire years in North American boreal forests. *Nature Climate Change*, *7*, 529–534. https://doi.org/10.1038/nclimate3329

Veraverbeke, S., Rogers, B. M., & Randerson, J. T. (2015). Daily burned area and carbon emissions from boreal fires in Alaska. *Biogeosciences*, *12*, 3579–3601. https://doi.org/10.5194/bg-12-3579-2015

Walker, X. J., Baltez, J., Cumming, S., Day, N., Johnsotne, J., Rogers, B., … Mack, M. (2018a). Soil organic layer combustion in boreal black spruce and jack pine stands of the Northwest Territories, Canada. *International Journal of Wildland Fire*, *27*, 125–134. https://doi.org/10.1071/wf17095

Walker, X. J., Rogers, B. M., Baltzer, J. L., Cummings, S. R., Day, N. J., Goetz, S. J., … Mack, M. C. (2018b). ABoVE: Wildfire carbon emissions at 30-m resolution, Northwest Territories, CA, 2014. ORNL DAAC, Oak Ridge, Tennessee, USA, https://doi.org/10.3334/ORNLDAAC/1561

Whitman, E., Parisien, M. A., Thompson, D. K., Hall, R. J., Skakun, R. S., & Flannigan, M. D. (2018). Variability and drivers of burn severity in the northwestern Canadian boreal forest. *Ecosphere*, *9*(2), e02128. https://doi.org/10.1002/ecs2.2128

SUPPORTING INFORMATION

Additional supporting information may be found online in the Supporting Information section at the end of the article.

How to cite this article: Walker XJ, Rogers BM, Baltzer JL, et al. Cross-scale controls on carbon emissions from boreal forest megafires. *Glob Change Biol*. 2018;00:1–15. https://doi.org/10.1111/gcb.14287